

# Quantum impurity coupled to Majorana edge fermions

Rok Žitko<sup>1</sup> and Pascal Simon<sup>2</sup>

<sup>1</sup>*Jožef Stefan Institute, Jamova 39, SI-1000 Ljubljana, Slovenia,*

*Faculty of Mathematics and Physics, University of Ljubljana, Jadranska 19, SI-1000 Ljubljana, Slovenia*

<sup>2</sup>*Laboratoire de Physique des Solides, CNRS UMR-8502, Université Paris Sud, 91405 Orsay Cedex, France*

(Dated: November 9, 2018)

We study a quantum impurity coupled to the edge states of a two-dimensional helical topological superconductor, i.e., to a pair of counter propagating Majorana fermion edge channels with opposite spin polarizations. For an impurity described by the Anderson impurity model, we show that the problem maps onto a variant of the interacting resonant two-level model which, in turn, maps onto the ferromagnetic Kondo model. Both magnetic and non-magnetic impurities are considered. For magnetic impurities, an analysis relying on bosonization and the numerical renormalization group shows that the system flows to a fixed point characterized by a residual  $\ln 2$  entropy and anisotropic static and dynamical impurity magnetic susceptibilities. For non-magnetic impurities, the system flows instead to a fixed point with no residual entropy and we find diamagnetic impurity response at low temperatures. We comment on the Schrieffer-Wolff transformation for problems with non-standard conduction band continua and on the differences which arise when we describe the impurities by either Anderson or Kondo impurity models.

PACS numbers: 73.20.-r, 72.10.Fk, 72.15.Qm, 75.30.Hx

## I. INTRODUCTION

Majorana fermionic operators are characterized by the relation  $\eta^\dagger = \eta$ , i.e., they represent particles which are their own antiparticles. A pair of Majorana (real) operators can be combined into one standard Dirac (complex) fermionic creation and one corresponding annihilation operator which operate within the Fock space of a single-level system. Majorana fermions can also be thought of as an equal linear combination of particles and holes. In recent years, a number of proposals have been advanced for physical realizations of condensed-matter systems having low-energy excitation spectra which can be formally described using Majorana fermion operators (see Refs. 1,2,3,4,5 for recent reviews). In such interacting many-particle systems Majorana fermions appear at low temperatures as emergent degrees of freedom. In particular, it has been argued that topological superconducting phases can be induced in topological insulators<sup>6–11</sup> by the proximity effect<sup>4,5,12–17</sup>. These phases are characterized by the presence of one or several Majorana excitation branches which are localized along the perimeter of the two-dimensional superconducting sheet. Such Majorana bands have energies inside the superconducting energy gap. In the absence of defects they are, in fact, the only excitations inside the gap. One distinguishes chiral topological superconductors with a single Majorana continuum which propagates in a unique direction (chirality) and helical topological superconductors with two Majorana continua which counter propagate and have opposite spin polarization (helicity or spin-momentum locking)<sup>4,18–21</sup>. While there is presently no confirmed physical realization of a helical topological superconductor, several recent theoretical proposals are based on heterostructures made from topological insulators (such as  $\text{Bi}_2\text{Se}_3$ ) and conventional superconductors (such as elemental superconducting metals). By tuning magnetic doping of the topological insulating layer, it should be in principle possible to obtain both chiral and helical topological superconductors<sup>21</sup>.

An important issue in this field is the fate of the Majorana fermions when electron-electron interactions are taken into account<sup>22,23</sup> and the role of disorder<sup>24–26</sup>, in particular that of impurities<sup>27</sup>. Dilute concentrations of impurities would lead to various measurable low-temperature anomalies due to the Kondo effect, while higher concentrations could even destabilize the edge states and qualitatively affect the behavior of the system. It is thus of considerable interest to accurately analyze the behavior of interacting impurities embedded near the edges of topological superconductors (TSC). This is particularly important because the doping of the topological insulator layer by magnetic impurities has been proposed as one of the methods to tune their material properties and to control their ground states. It is therefore likely that some magnetic dopant atoms will be invariably present at the edge area of the TSC, where the Majorana states are localized.

Since the impurities hybridize with the conducting states which have half the degrees of freedom of Dirac fermions (electrons), it is expected that there will be a number of particularities compared to the behavior of standard impurity models, such as the Anderson and Kondo impurity models. Furthermore, it is conceivable that one could attach quantum dots to such materials so that they would hybridize with the edge states of TSCs; such hybrid structures can also be described using the same class of impurity models.

In this work we study the Anderson impurity model with modified conduction-band and hybridization terms which only involve half the degrees of freedom of the standard model. In Sec. II, we describe the model and perform mappings to other known models. In Sec. III, we use bosonization techniques in order to gain some qualitative understanding about the expected behavior of the model. In Sec. IV, this analysis is complemented by a numerical analysis using a reliable non-perturbative technique, the numerical renormalization group (NRG), which allows to address both thermodynamic and dynamic properties of the system. By help of these two complementary studies, we show that the model ad-

mits two qualitatively different types of low-temperature fixed points, one associated with magnetic impurities (those with large electron-electron repulsion and occupancy near half-filling) which is characterized by  $\ln 2$  residual entropy and anisotropic magnetic response, and another associated with non-magnetic impurities (those with small electron-electron repulsion and/or occupancy away from half-filling) which is characterized by zero residual entropy and diamagnetic response. This is different from the standard Anderson impurity model where the low-temperature fixed point always belongs to the same family of Fermi-liquid fixed points and there are no discontinuities as a function of the model parameters (interaction strength, level energy, hybridization strength), only the quasiparticle scattering phase shifts are smoothly changed. In Sec. V, we perform the Schrieffer-Wolff transformation in the case of Majorana bands. We comment on the relations between the Anderson and Kondo impurity models in this generalized setting and compare our results of a magnetic impurity coupled to Majorana edge states with a recent study<sup>27</sup> which uses instead a Kondo Hamiltonian description. In particular, we find different results for the dynamical magnetic response and observe that the phase transition predicted in Ref. 27 does not show up when the impurity is instead properly described by a Anderson model. This is due to the fact that the phase transition predicted in Ref. 27 occurs for parameter values of a Kondo model which cannot arise from the Schrieffer-Wolff transformation of an Anderson model.

## II. MODEL AND MAPPINGS

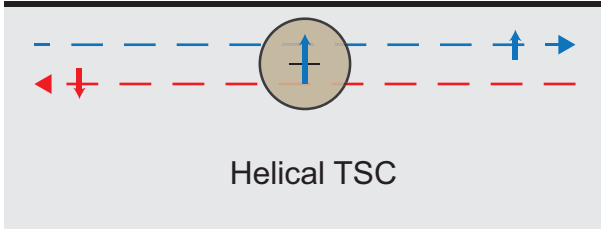


Figure 1. (Color online) Schematic representation of the single impurity problem studied in this work. A single impurity level (circle) is hybridized with two continua of counter-propagating Majorana fermions with opposite spin polarizations (dashed lines).

We study the single-impurity Anderson model (SIAM) consisting of an impurity (single orbital) coupled by hybridization to the edge states of a helical topological superconductor, i.e., to two continua composed of counter propagating Majorana particles with opposite spin polarization. The spin quantization axis is taken to be along the  $z$ -axis; the rotation symmetry in the spin space is broken in this model. The Hamiltonian can be obtained from the standard SIAM by projecting out half of the conduction-band degrees of freedom. A schematic representation is shown in Fig. 1. The Hamiltonian is

$$H = H_1 + H_2 + H_3, \quad (1)$$

where  $H_1$  is the impurity Hamiltonian

$$H_1 = \delta \sum_{\sigma} (n_{\sigma} - 1/2) + U(n_{\uparrow} - 1/2)(n_{\downarrow} - 1/2) + B_x(1/2)(d_{\downarrow}^{\dagger}d_{\uparrow} + d_{\uparrow}^{\dagger}d_{\downarrow}) \quad (2)$$

$$+ B_y(1/2)(id_{\downarrow}^{\dagger}d_{\uparrow} - id_{\uparrow}^{\dagger}d_{\downarrow}) \quad (3)$$

$$+ B_z(1/2)(n_{\uparrow} - n_{\downarrow}),$$

$H_2$  is the coupling Hamiltonian

$$H_2 = \sum_{k\sigma} V_k (\eta_{k\sigma} d_{\sigma} + d_{\sigma}^{\dagger} \eta_{k\sigma}), \quad (4)$$

and  $H_3$  is the conduction-band Hamiltonian for the Majorana modes

$$H_3 = \sum_{k>0} (vk\eta_{-k,\uparrow}\eta_{k,\uparrow} + v(-k)\eta_{-k,\downarrow}\eta_{k,\downarrow}). \quad (5)$$

The operators  $d_{\sigma}^{\dagger}$  with  $\sigma = \uparrow, \downarrow$  create an electron at the impurity level, and  $n_{\sigma} = d_{\sigma}^{\dagger}d_{\sigma}$  is the electron number (occupancy) operator. The parameter  $\delta = \epsilon + U/2$  measures the departure from the particle-hole symmetric point,  $\epsilon$  is the on-site energy,  $U$  is the electron-electron repulsion parameter, while  $B_x$ ,  $B_y$ , and  $B_z$  are the components of the external magnetic field applied on the impurity. The  $\eta_{k,\sigma}$  are Majorana fermions operators satisfying  $\eta_{k,\sigma}^{\dagger} = \eta_{-k,\sigma}$  and  $\{\eta_{-k,\sigma}, \eta_{k',\sigma'}\} = \delta_{kk'}\delta_{\sigma\sigma'}$ .  $v$  is the Fermi velocity. The hybridization is given by the matrix elements  $V_k$ . As common in the treatment of impurity models, we neglect the  $k$ -dependence of  $V_k$ , i.e.,  $V_k \equiv V$ ; this is permissible since we are mostly interested in the low-energy behavior of the system. We furthermore assume that  $V_k$  is real (see Appendix A for a generalization to complex  $V_k$  where we show that the phase of  $V_k$  determines the orientation of the privileged axis, to be discussed below, in the  $xy$  plane that is perpendicular to the spin-quantization axis of Majorana bands, i.e., the  $z$ -axis). The hybridization of the impurity with the conduction band is fully described by the hybridization energy scale  $\Gamma = \pi\rho|V|^2$ , where  $\rho$  is the density of states in the conduction band. In this work, we consider a constant density of states  $\rho = 1/\pi v$  so that  $\Gamma$  is a constant independent of energy.

It is important to note that in writing the Hamiltonian in the form of Eqs. (1-5) we have omitted terms which describe the coupling of the impurity to the bulk states of the superconductor which have energies above the superconducting gap. These modes can renormalize the effective parameters of the impurity Hamiltonian. For simplicity, we assume that these high-energy modes have already been integrated out and that the Hamiltonian  $H$  is an effective low-energy Hamiltonian valid on energy scales below the superconducting gap. The bandwidth of the Majorana modes thus equals twice the superconducting gap.

We now introduce the local Majorana operators  $\eta_{i\sigma}$  through

$$d_{\sigma} = \frac{1}{\sqrt{2}} (\eta_{1\sigma} + i\eta_{2\sigma}), \quad d_{\sigma}^{\dagger} = \frac{1}{\sqrt{2}} (\eta_{1\sigma} - i\eta_{2\sigma}), \quad (6)$$

$$\eta_{1\sigma} = \frac{1}{\sqrt{2}} (d_{\sigma} + d_{\sigma}^{\dagger}), \quad \eta_{2\sigma} = \frac{1}{\sqrt{2}i} (d_{\sigma} - d_{\sigma}^{\dagger}),$$

(note that we follow the normalization convention  $\eta_{i\sigma}^2 = 1/2$ ). The local spin and isospin operators can be expressed as

$$\begin{aligned}
s_x &= \frac{1}{2} (d_{\downarrow}^{\dagger} d_{\uparrow} + d_{\uparrow}^{\dagger} d_{\downarrow}) = \frac{i}{2} (\eta_{1\downarrow} \eta_{2\uparrow} + \eta_{1\uparrow} \eta_{2\downarrow}) \\
s_y &= \frac{1}{2} (i d_{\downarrow}^{\dagger} d_{\uparrow} - i d_{\uparrow}^{\dagger} d_{\downarrow}) = \frac{i}{2} (\eta_{1\downarrow} \eta_{1\uparrow} + \eta_{2\downarrow} \eta_{2\uparrow}) \\
s_z &= \frac{1}{2} (d_{\uparrow}^{\dagger} d_{\uparrow} - d_{\downarrow}^{\dagger} d_{\downarrow}) = \frac{i}{2} (-\eta_{1\downarrow} \eta_{2\downarrow} + \eta_{1\uparrow} \eta_{2\uparrow}) \\
i_x &= \frac{1}{2} (d_{\uparrow}^{\dagger} d_{\downarrow}^{\dagger} + d_{\downarrow} d_{\uparrow}) = \frac{i}{2} (\eta_{1\downarrow} \eta_{2\uparrow} - \eta_{1\uparrow} \eta_{2\downarrow}) \\
i_y &= \frac{1}{2} (i d_{\downarrow}^{\dagger} d_{\uparrow}^{\dagger} + i d_{\downarrow} d_{\uparrow}) = \frac{i}{2} (\eta_{1\downarrow} \eta_{1\uparrow} - \eta_{2\downarrow} \eta_{2\uparrow}) \\
i_z &= \frac{1}{2} (d_{\uparrow}^{\dagger} d_{\uparrow} + d_{\downarrow}^{\dagger} d_{\downarrow} - 1) = \frac{i}{2} (\eta_{1\downarrow} \eta_{2\downarrow} + \eta_{1\uparrow} \eta_{2\uparrow})
\end{aligned} \tag{7}$$

We rewrite  $H_1$  as

$$\begin{aligned}
H_1 &= \delta \sum_{\sigma} i \eta_{1\sigma} \eta_{2\sigma} + U \eta_{1\uparrow} \eta_{1\downarrow} \eta_{2\uparrow} \eta_{2\downarrow} \\
&\quad + B_x (i/2) (\eta_{1\downarrow} \eta_{2\uparrow} + \eta_{1\uparrow} \eta_{2\downarrow}) \\
&\quad + B_y (i/2) (\eta_{1\downarrow} \eta_{1\uparrow} + \eta_{2\downarrow} \eta_{2\uparrow}) \\
&\quad + B_z (i/2) (\eta_{1\uparrow} \eta_{2\uparrow} - \eta_{1\downarrow} \eta_{2\downarrow}),
\end{aligned} \tag{8}$$

while

$$H_2 = \sum_{k\sigma} V \sqrt{2} i \eta_{k\sigma} \eta_{2\sigma}. \tag{9}$$

Only the two  $\eta_{2\sigma}$  Majorana local modes are coupled to the continuum (hybridized). For  $\delta = B = U = 0$ , the two  $\eta_{1\sigma}$  modes are fully decoupled from the rest of the system. For  $U \neq 0$ , the  $\eta_{1\sigma}$  modes interact via the quartic term with the  $\eta_{2\sigma}$  modes. As we show in the following, this brings about non-trivial effects. For  $\delta = B = 0$  and finite  $U$ , we will see that on the temperature scale  $T_1 = f(U, \Gamma)$  the fluctuations of the  $\eta_{2\sigma}$  modes are frozen out and that the entropy is reduced by  $2 \times (1/2) \ln 2 = \ln 2$ . The  $\eta_{1\sigma}$  modes remain active, and the system has  $\ln 2$  residual entropy down to  $T = 0$ . We would therefore like to study the nature and the dynamics of this residual degree of freedom. We find that

$$i \eta_{1\downarrow} \eta_{1\uparrow} = s_y + i_y. \tag{10}$$

The residual degree of freedom thus corresponds to a mixed spin-isospin mode associated with a linear combination of spin and isospin projection operators along the  $y$  direction (see Appendix A for a generalization to an arbitrary phase factor in  $V_k$ ). For this reason we expect that the model has different magnetic response in the  $y$  direction as compared to the  $x$  and  $z$  directions. In the following, the privileged  $y$  direction will be referred to as the ‘‘longitudinal’’ direction, while the other two will be called ‘‘transverse’’ directions.

We now map the problem onto an interacting resonant two-level model. For that purpose, we introduce new Dirac

fermionic operators defined by

$$\begin{aligned}
a_k &= \frac{1}{\sqrt{2}} (\eta_{k\uparrow} + i \eta_{k\downarrow}), \\
a_k^{\dagger} &= \frac{1}{\sqrt{2}} (\eta_{-k\uparrow} - i \eta_{-k\downarrow}), \\
-ib &= \frac{1}{\sqrt{2}} (\eta_{2\uparrow} + i \eta_{2\downarrow}), \\
f &= \frac{1}{\sqrt{2}} (\eta_{1\uparrow} + i \eta_{1\downarrow}).
\end{aligned} \tag{11}$$

In terms of these operators,

$$\begin{aligned}
H_1 &= \delta (b^{\dagger} f + \text{H.c.}) - U (n_b - 1/2) (n_f - 1/2) \\
&\quad + B_x / 2 (i b^{\dagger} f^{\dagger} + \text{H.c.}) + B_z / 2 (b^{\dagger} f^{\dagger} + \text{H.c.}), \\
&\quad + B_y / 2 (1 - n_b - n_f)
\end{aligned} \tag{12}$$

$$H_2 = \sum_k V \sqrt{2} (a_k^{\dagger} b + \text{H.c.}), \tag{13}$$

$$H_3 = \sum_k v k a_k^{\dagger} a_k. \tag{14}$$

Notice that the summation in the last equation is indeed for all  $k$ . Here  $n_b = b^{\dagger} b$  and  $n_f = f^{\dagger} f$  are the occupancy operators for orbitals  $b$  and  $f$ , respectively. This is a variant of the interacting resonant two-level model for spinless Dirac fermions with *attractive* charge-charge coupling. The  $b$  mode directly hybridizes with the continuum, while the  $f$  mode is fully decoupled for  $\delta = U = B = 0$ . We note the similarity between the  $B_x$  and  $B_z$  terms in Eq. (12) (they differ essentially only by a phase shift of the operators), while  $B_y$  has a qualitatively different form. This is in line with the expected anisotropy of the system. The sum of the terms in  $B_x$  and  $B_z$  can be compactly rewritten as  $(B_{\perp} b^{\dagger} f^{\dagger} + \text{H.c.})/2$ , where

$$B_{\perp} = B_z + i B_x. \tag{15}$$

The interesting behavior results for non-zero parameters  $\delta$ ,  $U$ , and/or  $B$ . For finite interaction  $U$ , we expect to observe orthogonality catastrophe physics due to the effect of the occupancy changes at the impurity level  $f$  on the continuum.

In order to capture the physics associated with this model, let us first use a field-theoretical approach. This is the subject of the next section.

### III. BOSONIZATION APPROACH

A Hamiltonian somewhat similar to Eqs. (12-14) has been studied recently in the context of the charging of a narrow level in a quantum dot capacitively coupled to a broader one<sup>28-31</sup>. However, contrary to the Hamiltonian in Eq. (12), the levels in the dot were interacting via a repulsive Coulomb interaction, in which case the system always has a non-degenerate ground state and is a conventional Fermi liquid. Here, the interaction is attractive which, as we will see, can significantly change the physics.

We start with the case  $B_y = 0$ . We follow the bosonization procedure developed in Ref. 30 and repeat the main steps for

completeness. We first diagonalize the Hamiltonian  $H_2 + H_3$  which corresponds to a resonant-level model. The density of states of the level  $b$  corresponds to a Lorentzian of finite width  $\Gamma$  centered around zero energy. If we assume  $\delta, |B_\perp| \ll \Gamma$ , we can replace the density of states of the level  $b$  by a flat density<sup>30</sup> for energies  $\omega \in [-\pi\Gamma/2, \pi\Gamma/2]$  and 0 elsewhere, with height  $1/(\pi\Gamma)$ . In this limit, the energy scale  $\Gamma$  plays the role of an effective bandwidth. Therefore,  $H$  reads in the continuum and low-energy limit

$$H = -iv \int_{-\infty}^{\infty} \psi^\dagger(x) \partial_x \psi(x) dx - Ua : \psi^\dagger(0) \psi(0) : (n_f - 1/2) + \delta \sqrt{a} (\psi^\dagger(0) f + H.c.) + B_\perp \sqrt{a} (\psi^\dagger(0) f^\dagger + H.c.), \quad (16)$$

where  $a \sim 2v/\Gamma$  is a new UV cut-off associated with the new effective bandwidth  $\Gamma$ ,  $\psi(x)$  is a right-moving field associated with the diagonalization of the low-energy limit of  $H_2 + H_3$ . The Hamiltonian in Eq. (16) can be treated using bosonization. We introduce a bosonic field associated to the chiral fermionic one  $\psi(x) \approx \frac{1}{2\pi a} e^{-i\phi(x)}$ , such that

$$H = v \int_{-\infty}^{\infty} \frac{dx}{4\pi} (\nabla\phi)^2 - v \frac{2\alpha_U}{\pi} \nabla\phi(0) (n_f - 1/2) + \frac{\delta}{\sqrt{2}} (e^{i\phi(0)} f + H.c.) + \frac{B_\perp}{\sqrt{2}} (e^{i\phi(0)} f^\dagger + H.c.), \quad (17)$$

where

$$\alpha_U = \arctan(U/2\Gamma) \quad (18)$$

is fixed so that the phase shift we obtain for  $\delta = B_\perp = 0$  in the fermionic representation equals the one calculated in the bosonic representation for a given occupation of the  $f$  level.<sup>30</sup> Next, we apply the canonical transformation  $H' = U^\dagger H U$  with

$$U = \exp[i(2\alpha_U/\pi)\phi(0)(n_f - 1/2)], \quad (19)$$

such that

$$H' = v \int_{-\infty}^{\infty} \frac{dx}{4\pi} (\nabla\phi)^2 + \frac{\delta}{\sqrt{2}} (e^{i\gamma_+ \phi(0)} f + H.c.) + \frac{B_\perp}{\sqrt{2}} (e^{i\gamma_- \phi(0)} f^\dagger + H.c.), \quad (20)$$

where we have introduced

$$\gamma_\pm = 1 \pm 2\alpha_U/\pi. \quad (21)$$

Let us first consider the following two situations:  $\delta \neq 0, B_\perp = 0$  and  $\delta = 0, B_\perp \neq 0$ . In both cases, the Hamiltonian in Eq. (20) maps to a bosonized formulation of the anisotropic Kondo model

$$H_{AK} = \sum_{k\sigma} \epsilon_k c_{k\sigma} c_{k\sigma} + \sum_{kk'\sigma'} J_i \mathbf{S}^i \sigma_{\sigma\sigma'}^\dagger c_{k\sigma}^\dagger c_{k'\sigma'}, \quad (22)$$

where  $\epsilon_k = vk$  and  $\sigma^i$  are the Pauli matrices ( $i = x, y, z$ ). The Kondo couplings  $J_i$  are such that  $J_x = J_y = J_\perp$ . The bosonization of (22), as derived in Refs. 32,33, provides the identification

$$\begin{aligned} \delta &= J_\perp / \sqrt{8} \\ \gamma_\pm &= \sqrt{2} \left[ 1 - \frac{2}{\pi} \arctan(\pi\rho J_z/4) \right], \end{aligned} \quad (23)$$

where  $\rho$  is the density of states in the large- $\Gamma$  limit we are considering. In the limit where  $\Gamma$  is much larger than  $U$ , we can linearize the arctan functions and estimate

$$J_z \approx \pi\Gamma(2 - \sqrt{2}) \mp \sqrt{2}U. \quad (24)$$

The upper sign ( $-$ ) corresponds to the case  $\delta \neq 0, B_\perp = 0$ , and the lower sign ( $+$ ) to the case  $\delta = 0, B_\perp \neq 0$ . Let us now discuss both cases separately.

*Case  $\delta \neq 0$  and  $B_\perp = 0$ .* – We see from Eq. (24) that a large  $U \gg \Gamma$  enforces  $J_z < 0$ , *i.e.*, a ferromagnetic Kondo model, while a small  $U$  leads to an antiferromagnetic Kondo model. In the latter case, we can extract a Kondo scale  $T_K^+$  associated with the screening of the magnetic moment. From the known results on the anisotropic Kondo model,<sup>34</sup> we find

$$T_K^+ \sim \Gamma \left( \frac{\delta}{\Gamma} \right)^{\frac{2}{2-\gamma_+^2}}, \quad (25)$$

with  $\gamma_+$  defined in Eq. (21). We remind that this result makes sense only for  $J_z > 0$  (small- $U$  case).

In order to estimate the low energy physics in the presence of both  $\delta$  and  $U$  terms, we can rely on the lowest order renormalization group (RG) equations for the Kondo model<sup>33</sup>

$$\frac{dJ_\perp}{dl} = \rho J_\perp J_z - \rho^2 J_\perp (J_\perp^2 + J_z^2)/4 \quad (26)$$

$$\frac{dJ_z}{dl} = \rho J_\perp^2 - \rho^2 J_z J_\perp^2/2, \quad (27)$$

where  $l$  is a running length scale. In particular, if we neglect the cubic terms, this is the standard Kosterlitz-Thouless RG flow where  $J_z^2 - J_\perp^2$  is a constant of the flow. When  $J_z < 0$ , the infrared fixed point depends on whether  $|J_z(a)|$  is above or below the separatrix  $J_\perp = -J_z$ , assuming  $J_\perp > 0$ . If  $|J_z(a)| > J_\perp(a)$ , the fixed point is a strong-coupling one which corresponds to the antiferromagnetic Kondo fixed point and the formation of a Kondo singlet. However, for  $|J_z(a)| < J_\perp(a)$ , the flow is driven toward a fixed line corresponding to  $J_\perp \rightarrow 0$  and  $J_z \rightarrow J_z^* < 0$  associated with the ferromagnetic Kondo model and therefore an unscreened free moment. Although we have assumed  $\Gamma$  to be larger than other scales, the condition  $J_\perp(a) > |J_z(a)|$  associated with a Fermi-liquid fixed point and a screened magnetic moment translates into

$$\delta > U/2 - \frac{\pi(\sqrt{2}-1)}{2}\Gamma. \quad (28)$$

*Case  $\delta = 0$  and  $B_\perp \neq 0$ .* – This case is simpler since  $J_z > 0$  for all values of  $U$ . Therefore, the low energy physics

is described by a Fermi liquid fixed point with a screened magnetic moment and we can define a Kondo scale  $T_K^-$  by

$$T_K^- \sim \Gamma \left( \frac{B_\perp}{\Gamma} \right)^{\frac{2}{2-\gamma_-^2}}, \quad (29)$$

with  $\gamma_-$  defined in Eq. (21).

*General case.* – When both  $\delta$  and  $B_\perp$  are different from zero, the mapping to the anisotropic Kondo problem breaks down. However, at small  $U$  compared to  $\Gamma$ , both terms independently favor a strong-coupling fixed point with a screening of the local moment. Therefore, we expect the same behavior in the presence of both terms. In the large- $U$  limit with  $B_\perp = 0$ , a ferromagnetic Kondo model is favored and a local moment is stabilized. The addition of a small magnetic field  $B_\perp$  around this fixed point is, however, a relevant perturbation which destabilizes this behavior and a non-magnetic fixed point is also expected.

In our analysis, we have considered  $B_y = 0$ . However, we can extend the previous bosonization analysis to models with  $B_y \neq 0$ . The term  $B_y$  has two effects: First, it provides an additional potential scattering term  $-B_y a/2 : \psi(0)\psi(0) :$  in the continuum-limit Hamiltonian in Eq. (16) which will modify the phase-shift analysis. Second, it adds an extra term  $-B_y(n_f - 1/2)/2$  which corresponds to a magnetic field of the form  $-B_y S^z/2$  in the equivalent Kondo Hamiltonian in Eq. (22). As discussed above, the latter term would polarize a free local moment and no residual entropy is expected at energy below this magnetic field.

#### IV. NUMERICAL RENORMALIZATION GROUP ANALYSIS

We now study the Hamiltonian in its original (non-transformed) form of Eq. (1) using the numerical renormalization group (NRG) method<sup>35–37</sup>. This technique is essentially an iterative exact diagonalization of an appropriately discretized form of the Hamiltonian, where at each partial diagonalization step the high-energy excitations are discarded (“truncated”) and only the low-energy part of the spectrum is retained in the subsequent calculation steps. This approximation is appropriate because the matrix elements coupling levels with widely different energy scales are small<sup>35</sup>. The NRG method has already been applied to problems involving an impurity coupled to Majorana edge fermions; for details, see Ref. 38. (In this work, the NRG calculations have mostly been performed using parameters  $\Lambda = 3$ ,  $E_{\text{cutoff}} = 10$  or at most 5000 states, whichever is lower,  $N_z = 4$ ,  $\alpha = 0.6$ .)

##### A. Thermodynamic properties: particle-hole symmetric case

We first study the problem for a particular choice of  $\delta = 0$ , i.e., we focus on the particle-hole (p-h) symmetric problem. We will show in the following that there is actually a finite region in the  $(\delta, U, \Gamma)$  parameter space where the problem flows to the same type of the low-temperature fixed point as along

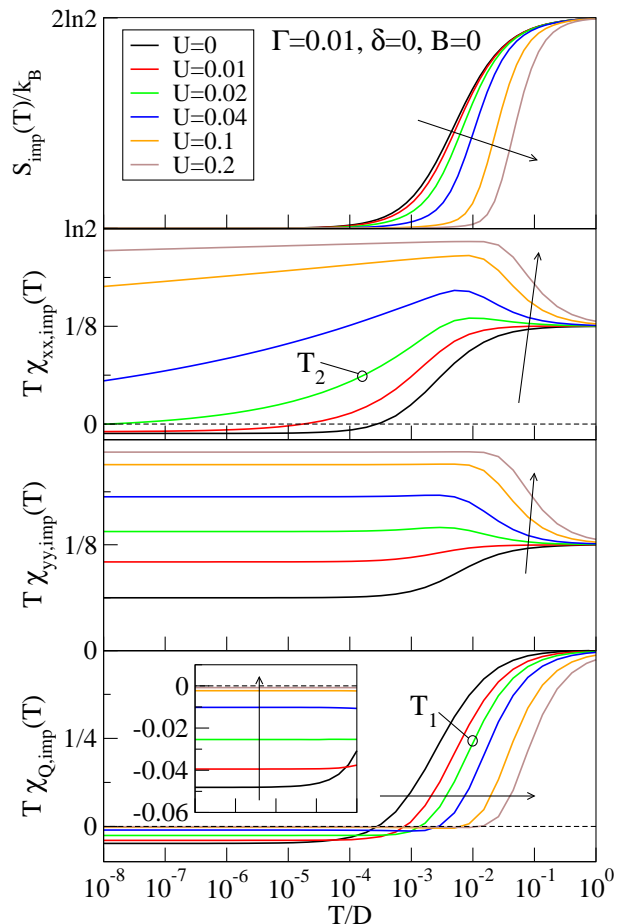


Figure 2. (Color online) Thermodynamic properties (impurity entropy and impurity susceptibilities) at the particle-hole symmetric point  $\delta = 0$  for a range of values of the interaction strength  $U$ . The arrows indicate the direction of increasing  $U$ . In the absence of the external magnetic field, one has  $\chi_{xx,\text{imp}} = \chi_{zz,\text{imp}}$  due to symmetry. The off-diagonal magnetic susceptibilities are all zero. On the curves for  $U = 0.02$ , we label the positions of the temperatures  $T_1$  and  $T_2$  (see the main text for their definitions).

the p-h symmetric line, thus the results are more general. The impurity entropy and thermal spin and charge susceptibilities are shown in Fig. 2 for a range of the interaction strengths  $U$ , including for the non-interacting  $U = 0$  limit. We remind the reader that the impurity entropy quantifies the number of the effective degrees of freedom  $p$  on the impurity via

$$S_{\text{imp}}(T) = k_B \ln p(T). \quad (30)$$

The impurity magnetic susceptibility corresponds to the effective local magnetic moment as

$$\mu_i^2(T) = T \chi_{ii,\text{imp}}(T), \quad (31)$$

where

$$T \chi_{ij,\text{imp}}(T) = \langle S_i S_j \rangle - \langle S_i \rangle \langle S_j \rangle, \quad (32)$$

with  $S_i$  the  $i$ -component of the total spin of the system. Here  $\langle \rangle_0$  denotes the expectation value for a system without the impurity. Finally, the impurity charge susceptibility  $\chi_{Q,\text{imp}}$  is

defined through

$$T\chi_{Q,\text{imp}}(T) = \langle Q^2 \rangle - \langle Q \rangle^2 \quad (33)$$

where  $Q$  is the total charge in the system. Since the impurity susceptibility is defined as the difference between an expectation value in the full system and the expectation value in the system without the impurity (i.e., the impurity contribution to the total system susceptibility), the impurity susceptibilities can be negative. This is different from the local susceptibilities of the impurity, which are different quantities that are positive-definite.

In the high-temperature limit, the system behaves as the standard SIAM in the same limit<sup>36</sup>: the impurity freely fluctuates between all four possible states, thus the entropy is  $\ln 4$ , while the magnetic moment is  $(0 + 1/4 + 1/4 + 0)/4 = 1/8$ , since only two of the four states have magnetic moment of  $1/4$ . The charge moment  $T\chi_{Q,\text{imp}}$  is  $1/2$  due to maximal charge fluctuations on the impurity.

On the temperature scale  $T_1 \approx \max(U, \Gamma)$ , the directly coupled Majorana modes  $\eta_{2\sigma}$  are frozen out (or, which is equivalent, the Dirac mode  $b$  is frozen out) and we enter a  $\ln 2$  plateau in the impurity entropy which persists down to  $T = 0$ . The freezing-out of the charge degrees of freedom is also reflected in the effective charge moment  $T\chi_{Q,\text{imp}}(T)$ , which on the temperature scale  $T_1$  drops to some small (negative) value and remains constant down to  $T = 0$ . The larger  $U$  is, the larger is the reduction of the charge fluctuations on the impurity, and the closer does the charge moment approach to zero. We emphasize that in the standard SIAM the effective charge susceptibility goes to zero at low temperatures and it is always positive.

The residual  $\ln 2$  entropy suggests that the other two Majorana modes  $\eta_{1\sigma}$  (i.e., the Dirac mode  $f$ ) remain decoupled; this is strictly true only for the non-interacting  $U = 0$  model, see Eq. (12), but an effective decoupling also occurs for  $U \neq 0$ . The magnetic susceptibility curves indicate, however, that the behavior within the  $\ln 2$  entropy plateau is not trivial, see the two middle panels in Fig. 2. The most striking feature is the strongly anisotropic behavior: while the effective moments in the transverse  $x$  and  $z$  directions are reduced (“screened”) at low temperatures, the longitudinal ( $y$ -axis) effective moment reaches its asymptotic value on the temperature scale of  $T_1$  and remains constant down to  $T = 0$ . We also observe that the behavior is different depending on the value of the ratio  $U/\Gamma$ . (We remind the reader that this same ratio controls the stability of the non-magnetic solution of the Hartree-Fock equations for the standard SIAM. For  $U/\pi\Gamma < 1$  the paramagnetic solution is stable, while for  $U/\pi\Gamma > 1$  the solution breaks the spin symmetry and the Hartree-Fock approximation is no longer applicable. This ratio thus determines whether the system is in the “Kondo regime” or not.)

Let us first consider the case of large  $U$ , i.e.,  $U/\Gamma \gtrsim 1$ , which corresponds to the magnetic regime. The transverse magnetic susceptibility indicates a progressive reduction of the effective impurity magnetic moment. This reduction occurs at some low temperature scale  $T_2$  which appears to be exponential in  $U/\Gamma$ , similar to the exponential behavior of the

Kondo temperature in the standard SIAM. The scale  $T_2$  may be defined, somewhat arbitrarily, through  $\mu_x^2(T_2) = \mu_x^2(T = \infty)/2 = 1/8$ . The temperature  $T_2$  is plotted as a function of  $U/\Gamma$  in Fig. 3. We find an excellent fit to the function

$$T_2 = c_1 U \exp \left[ -c_2 \left( \frac{U}{\Gamma} \right)^2 \right], \quad (34)$$

where  $c_1 = 3.73$  and  $c_2 = 0.78 \approx \pi/4$ . This is distinctly different from the expression for the Kondo temperature in the standard SIAM which takes the form  $T_K \sim U \exp(-\pi U/8\Gamma)$ . The scale  $T_2$  appears to be in many respects similar to the low-energy scale studied in Ref. 30, although the dependence on the parameters is exponential rather than algebraic. The physical mechanism which controls the scale  $T_2$  is not clear at present.

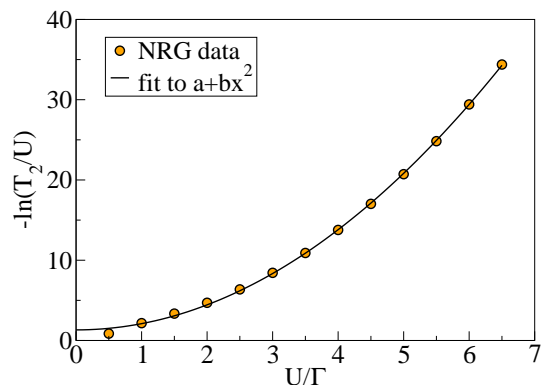


Figure 3. (Color online) The temperature  $T_2$  where the effective transverse magnetic moment  $\mu_x^2 = T\chi_{xx,\text{imp}}(T)$  is reduced to  $1/8$ . The full curve is a fit which corresponds to Eq. (34).

Note that at zero temperature the impurity spin is not screened in the usual sense (which would be associated with a reduction of the impurity entropy to zero due to the formation of a non-degenerate spin-singlet Kondo state). In particular, the effective longitudinal moment is still non-zero, thus the spin is maximally anisotropic; it behaves as an Ising spin which cannot rotate away from the  $y$  direction.

For small  $U$  of order  $\Gamma$ , we find somewhat different behavior. In this case, the scales  $T_2$  and  $T_1$  are not well separated: the charge and spin susceptibilities are reduced simultaneously. Again, the system has residual  $\ln 2$  entropy and there is residual longitudinal magnetic moment.

In analogy with the standard SIAM, we find that the interaction strength  $U$  plays the role of the effective bandwidth<sup>36</sup>, so that for constant  $U/\Gamma$  ratio the thermodynamic curves are simply shifted to lower energy scales proportionally to  $U$ . Finally, it should also be remarked that at the particle-hole symmetric point, the low-temperature stable fixed point of the system is exactly the same irrespective of the values of the parameters  $U$  and  $\Gamma$ ; again, a similar feature is also found in the standard SIAM<sup>36</sup>.

It is interesting to note that the second scale  $T_2$  does not very clearly appear in the renormalization-group energy-level flow diagram, Fig. 4, which is consistent with the constancy

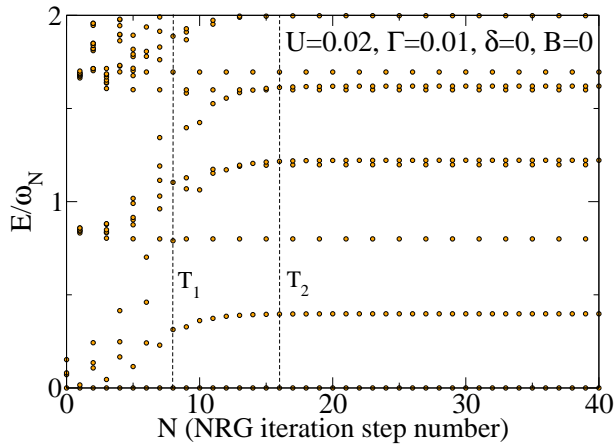


Figure 4. Renormalization-group flow diagram. The NRG iteration step numbers corresponding to the temperature scales  $T_1$  and  $T_2$  are indicated.

of  $S_{\text{imp}}$  at low temperatures. The fact that the susceptibility curves nevertheless exhibit temperature dependence then implies that it is the nature of the low-energy excitations which changes with the temperature. There are no conserved quantum numbers in the problem, thus the information about the spin susceptibility is contained in the matrix elements, such as  $\langle i|S_z|j\rangle$ , between the energy eigenstates. These matrix elements do have an RG flow. At the particle-hole symmetric point the system has double degeneracy (in fact the ground state and the low-energy excitations are all doubly degenerate). For  $\delta = B = 0$ , this is a direct consequence of the system being non-ergodic, but the double degeneracy is also found for  $\delta \neq 0$  (see also below), where the system is, in fact, ergodic. While the  $\delta = B = 0$  regime is in some sense pathological, we find that the behavior of the system varies smoothly as these parameters are varied from 0, therefore the results of the NRG calculations for  $\delta = B = 0$  are also physically relevant in spite of the system being, strictly-speaking, non-ergodic.

### B. Thermodynamic properties: asymmetric case

In the magnetic regime ( $U/\Gamma \gtrsim 1$ ), the departure from the particle-hole (p-h) symmetric point does not affect the behavior as long as

$$|\delta| < U/2 - c\Gamma, \quad (35)$$

where  $c$  is a number of order 1, at which point the fixed point is destabilized, see Fig. 5. Notice that a similar condition was found in the bosonization approach [see Eq. (28)] even though the analysis was based on a large- $\Gamma$  limit. This condition is similar to the region of existence of the “magnetic” local-moment fixed point in the standard SIAM<sup>36,39</sup>. In the weak-interaction regime ( $U/\Gamma \lesssim 1$ ), the magnetic fixed point is only stable in the immediate vicinity of the p-h symmetric point and the residual entropy is released at low temperatures even for small  $\delta$ . There thus exists a two-dimensional sheet of

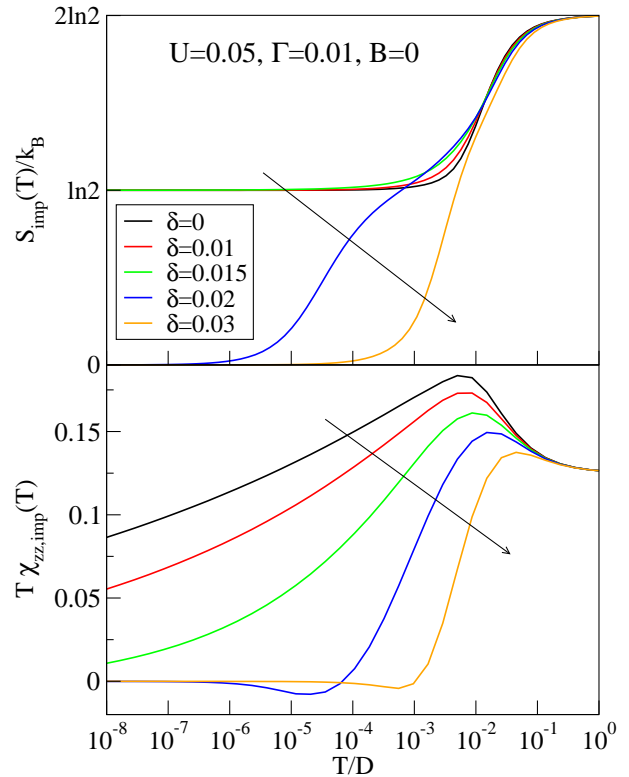


Figure 5. (Color online) Thermodynamic behavior away from the particle-hole symmetric point at  $\delta = 0$ . The arrows indicate the direction of increasing  $\delta$ . The transition point corresponds to  $|\delta| \sim U/2 - c\Gamma$  with  $c$  of order 1.

transition points in the  $(\delta, U, \Gamma)$  parameter space which separates the regimes with or without the residual entropy. The quantum phase transition is of the Kosterlitz-Thouless type; the cross-over between the magnetic and non-magnetic fixed point occurs on a temperature scale which is an exponential function of  $\delta - \delta_c$ , where  $\delta_c$  is the critical value of the parameter. A numerically determined phase diagram is shown in Fig. 6. We emphasize again that the existence of a phase transition is significantly different from the behavior of the standard SIAM, where the variation of the system properties in the  $(\delta, U, \Gamma)$  space is smooth and we merely move along a line of Fermi-liquid fixed points parameterized by the quasi-particle scattering phase shift.

By changing the on-site energy  $\delta$ , we tune the level occupancy  $n$ . The occupancy operator  $n$  is trivially related to the  $z$ -component of the isospin (also known as the axial charge) operator  $i_z = 1/2(n-1)$ , see Eq. (7). In this section, we have thus established that the magnetic fixed point is stable with respect to the non-zero isospin field  $i_z$ . Due to the symmetry of the problem, this implies that the system is also stable with respect to moderately large isospin field  $i_x$ , which can be induced by the superconducting proximity effect. We find, however, that non-zero isospin field  $i_y$  will drive the system to the non-magnetic fixed point on the energy scale of  $i_y$ .

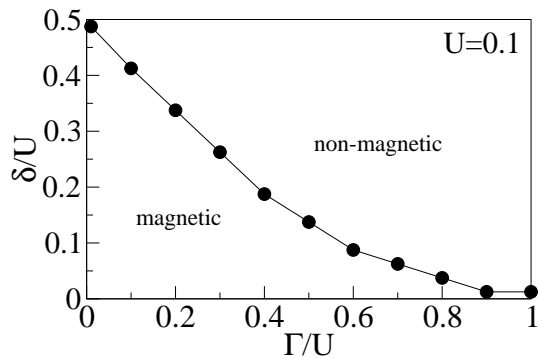


Figure 6. Phase diagram in the  $(\Gamma, \delta)$  plane for fixed interaction parameter  $U$ .

### C. Effects of the magnetic field

In the presence of an external magnetic field, the entropy is released and the effective moment goes to zero at low temperatures, see Fig. 7. The effect of the field is direction dependent. For a field along the “longitudinal”  $y$  direction, the entropy is always released on the temperature scale of  $B_y$ . For a field along the “transverse”  $x$  and  $z$  directions the behavior depends on the  $U/\Gamma$  ratio, in other words, it depends on whether the impurity is magnetic or not. For a magnetic impurity (large  $U/\Gamma$  ratio) the entropy is released on the temperature scale of  $|B_\perp|$ , while for a non-magnetic impurity (small  $U/\Gamma$  ratio) this only happens on a much reduced temperature scale, see Fig. 7. This behavior is described by the Kondo scale  $T_K^-$  defined in Eq. (29), although the parameters  $B_\perp$  and  $\Gamma$  need to be rescaled by some constant factors in order to obtain full numerical agreement.

The zero-temperature dynamical magnetic susceptibility curves for zero and non-zero magnetic field along transverse and longitudinal directions are shown in Fig. 8. In the absence of the field, the magnetic susceptibility in the transverse directions diverges at  $\omega = 0$ , while the longitudinal susceptibility goes to zero. All components of the magnetic susceptibility also feature a peak on the frequency scale of the atomic energies (at  $\sim U$ , if we are in the Kondo regime, see Figs. 8). In standard SIAM, the magnetic susceptibility peaks at  $T_K$  and goes to zero at small frequencies as a linear function of  $\omega$ , as mandated by the Korringa relation for Fermi-liquid systems<sup>40</sup>; the susceptibility curve also has a peak at  $\omega \sim U/2$ .

In the presence of a transverse magnetic field  $B_x$ , all components of the magnetic susceptibility tensor peak on the scale of the magnetic field and then go to zero. This is even true for the longitudinal susceptibility which in the absence of the field goes to zero. For longitudinal magnetic field  $B_y$ , the transverse components of the magnetic susceptibility peak on the scale of the magnetic field, while the longitudinal susceptibility peaks on the same scale as in the absence of the field and no further peak emerges at  $\omega \sim B_y$ . These features of the magnetic response of the system are characteristic for impurities coupled to helical Majorana edge states and clearly distinct from that of the standard SIAM. We also note that the results do not seem to agree with those found for an equiva-

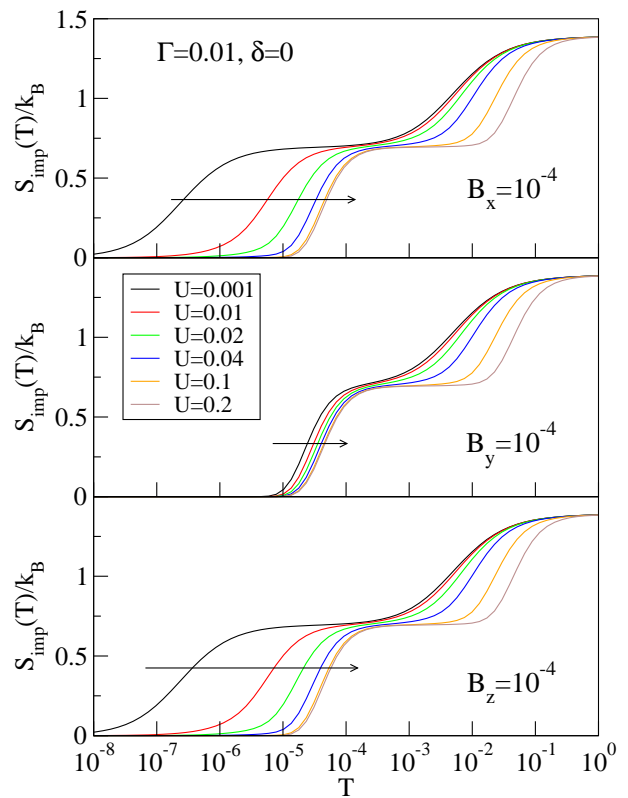


Figure 7. (Color online) An impurity in an external magnetic field along  $x$ ,  $y$ , and  $z$  directions, respectively, with constant strength  $|\mathbf{B}|$ . For each direction of the field, the parameter  $U$  is swept from the weak-interaction to the strong-interaction (Kondo) regime. The arrows indicate the direction of increasing  $U$ .

alent Kondo impurity problem in Ref. 27. The difference can be explained in part by the fact that the Anderson and Kondo impurity models are not fully equivalent; see Sec. V.

### D. Spectral functions

The zero-temperature spectral functions of the impurity are shown in Fig. 9. In addition to the charge-fluctuation peaks at  $\omega \sim U/2$ , as in the standard SIAM, one observes a sharp resonance on the scale of  $T_2$  with an inverse-power-law shape, i.e., the spectral function diverges. (Of course, one cannot attach a scale to a power-law function. Instead,  $T_2$  roughly corresponds to the energy where the cross-over to the power-law behavior occurs.) This inverse-power-law divergence replaces the Kondo resonance of the standard SIAM, which at the lowest energy scales looks like a parabolic peak and is finite. For strictly decoupled Majorana modes one would expect a delta peak at zero frequency; the “broadening” into the inverse-power-law peak is thus an interaction effect related to the Anderson orthogonality catastrophe physics. The exponent depends on the interaction strength, see the inset in Fig. 9. We find that the exponent  $\alpha$  is well fitted by  $\alpha = 1 - \frac{2}{\pi} \arctan(U/4\Gamma)$ .

We also observe that the anomalous spectral functions are



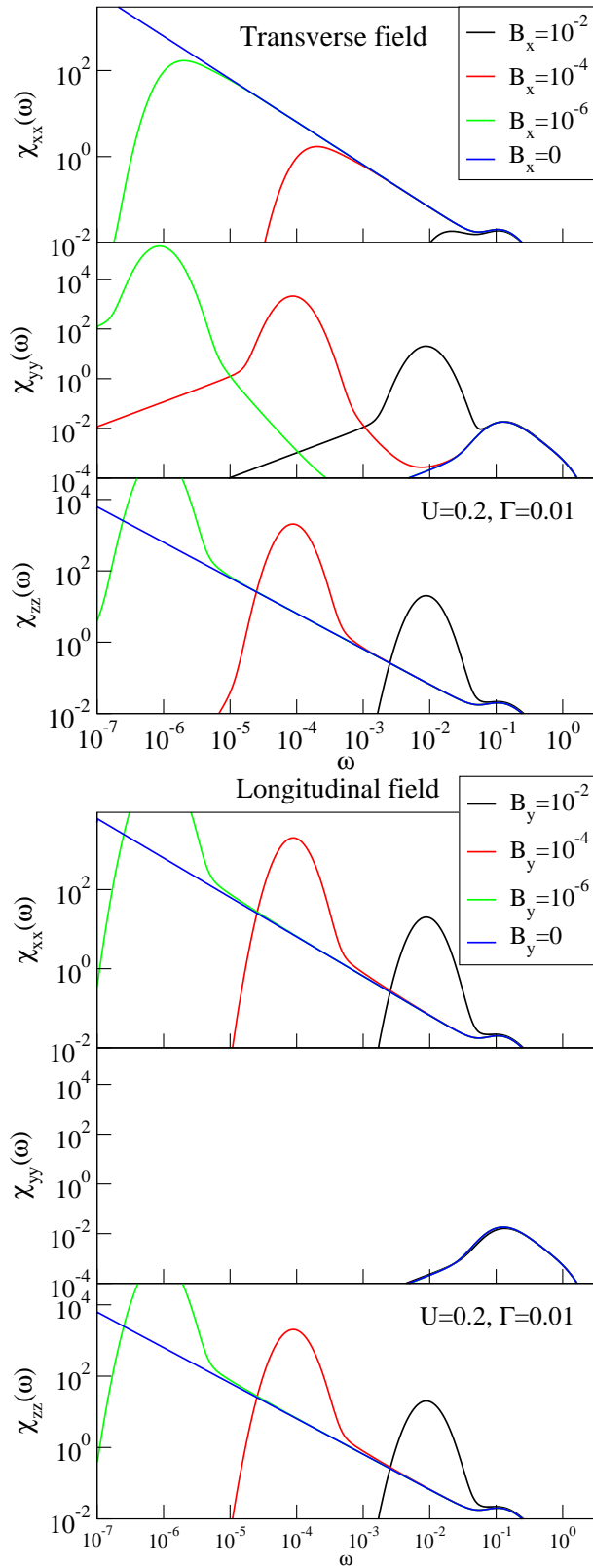


Figure 8. (Color online) Dynamical magnetic susceptibility functions for an external magnetic field applied along the transverse ( $x$ ) direction (top panels) and along the longitudinal ( $y$ ) direction (bottom panels).

non-zero, which is expected for an impurity coupled to a superconductor.

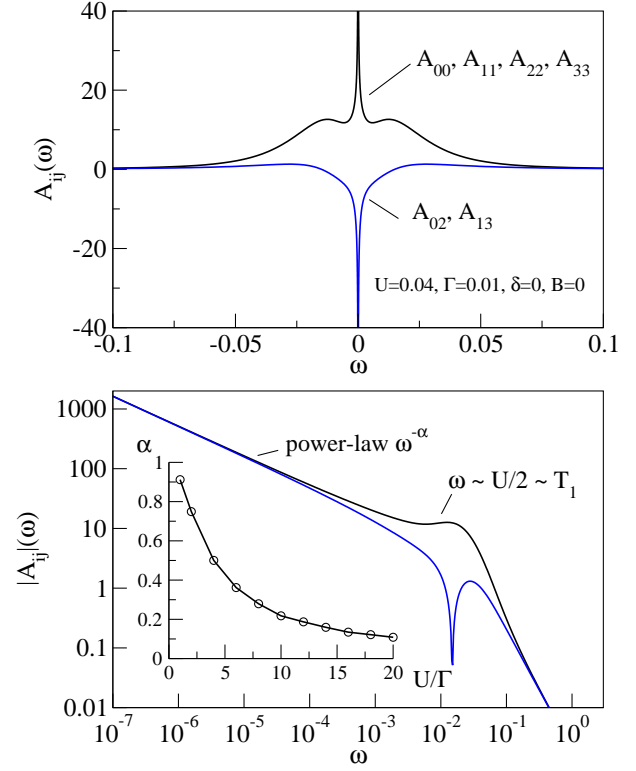


Figure 9. (Color online) Spectral properties of the impurity. The non-zero spectral functions are shown. We introduce the notation  $d_0 = d_{\downarrow}^{\dagger}$ ,  $d_1 = d_{\uparrow}^{\dagger}$ ,  $d_2 = d_{\downarrow}$ ,  $d_3 = d_{\uparrow}$  and define the spectral functions as  $A_{ij}(\omega) = -(1/\pi)\text{Im}\langle\langle d_i; d_j^{\dagger} \rangle\rangle_{\omega+i\delta}$ . Non-zero anomalous spectral functions  $A_{02}$  and  $A_{13}$  thus indicate the presence of pairing correlations. The inset in the bottom panel represents the power-law exponent as a function of the interaction strength.

## V. SCHRIEFFER-WOLFF TRANSFORMATION

We now consider a generalization of the Hamiltonian  $H$  defined in Eqs. (1-5). We take the conduction-band Hamiltonian as in the standard SIAM:

$$H'_3 = \sum_{k\sigma} \epsilon_k c_{k\sigma}^{\dagger} c_{k\sigma}. \quad (36)$$

This conduction band has twice the number of the degrees of freedom as that described by Eq. (5) since there are now two Majorana modes at each  $k$ :  $\eta_{k1\sigma}$  and  $\eta_{k2\sigma}$ . The Majorana and Dirac modes are related by

$$\begin{aligned} c_{k\sigma} &= \frac{1}{\sqrt{2}} (\eta_{k1\sigma} + i\eta_{k2\sigma}), & c_{k\sigma}^{\dagger} &= \frac{1}{\sqrt{2}} (\eta_{k1\sigma} - i\eta_{k2\sigma}) \\ \eta_{k1\sigma} &= \frac{1}{\sqrt{2}} (c_{k\sigma} + c_{k\sigma}^{\dagger}), & \eta_{k2\sigma} &= \frac{1}{i\sqrt{2}} (c_{k\sigma} - c_{k\sigma}^{\dagger}). \end{aligned} \quad (37)$$

The hybridization term allows for unequal coupling of the Majorana components:

$$H'_2 = \alpha \sum_{k\sigma} V_k (\eta_{k1\sigma} d_\sigma + d_\sigma^\dagger \eta_{k1\sigma}) / \sqrt{2} + \beta \sum_{k\sigma} V_k (-i\eta_{k2\sigma} d_\sigma + i d_\sigma^\dagger \eta_{k2\sigma}) / \sqrt{2}, \quad (38)$$

where  $\alpha$  and  $\beta$  are some real numbers. For  $\alpha = \beta = 1$ , this is the standard SIAM, while for  $\alpha = 0, \beta = 1$  we recover the Majorana SIAM studied in this work (up to some differences in the notation and a factor of  $\sqrt{2}$  in the definition of  $V_k$ ). We can thus smoothly interpolate between the two limiting cases. In the following, for reasons of simplicity we assume  $V_k$  to be independent of  $k$ , i.e.,  $V_k \equiv V$ .

We now proceed to perform the Schrieffer-Wolff transformation<sup>41,42</sup> for the generalized Anderson impurity model in the large- $U$  limit in order to derive an effective Kondo model. The low-energy subspace consists of those many-particle states where the impurity is singly occupied, and we denote by  $P_0$  the projection operator onto this subspace. Then  $Q_0 = 1 - P_0$  is the projector onto the orthogonal (“high-energy”) subspace. We introduce the superoperator

$$\mathcal{O}(X) = P_0 X Q_0 + Q_0 X P_0. \quad (39)$$

We find that  $\mathcal{O}(H'_2) = H'_2$ , thus  $H'_2$  is a block-off-diagonal operator. We next introduce the superoperator

$$\mathcal{L}(X) = \sum_{i,j} \frac{\langle i | \mathcal{O}(X) | j \rangle}{E_i - E_j} |i\rangle \langle j| - \text{H.c.} \quad (40)$$

Here  $\{|i\rangle\}$  is an orthonormal basis of  $H_0 = H_1 + H'_3$  such that  $H_0|i\rangle = E_i|i\rangle$ . We assume that the states  $|i\rangle$  in Eq. (40) belong to the low-energy subspace, while  $|j\rangle$  belong to the high-energy subspace (the  $-\text{H.c.}$  term then generates the remaining terms). To lowest order in hopping  $aV$ , one has

$$S = \mathcal{L}(H'_2) + O(V^2), \quad (41)$$

and

$$H_{\text{eff}} = H_0 P_0 + \frac{1}{2} P_0 [S, H'_2] P_0 + O(V^4). \quad (42)$$

We find

$$\mathcal{L}(H'_2) = \sum_{\sigma, \gamma, \{k_i\}, \{k_j\}} \frac{\langle \sigma \{k_i\} | H_2 | \gamma \{k_j\} \rangle}{E_{\sigma \{k_i\}} - E_{\gamma \{k_j\}}} |\sigma \{k_i\}\rangle \langle \gamma \{k_j\}| - \text{H.c.}, \quad (43)$$

where  $\sigma \in \{\uparrow, \downarrow\}$  indexes the impurity states in the low-energy subspace,  $\gamma \in \{0, 2\}$  indexes the impurity states in the high-energy subspace, while  $\{k_i\}$  and  $\{k_j\}$  are the occupancies of the conduction-band states. All terms in  $H'_2$  are such that the sets  $\{k_i\}$  and  $\{k_j\}$  must differ by the occupancy

of a single level. We obtain

$$S = \sum_{k\sigma} \frac{(\beta - \alpha)V/2}{\epsilon_k + \epsilon} (1 - n_{-\sigma}) c_{k\sigma}^\dagger d_\sigma^\dagger - \text{H.c.} + \sum_{k\sigma} \frac{(\alpha + \beta)V/2}{\epsilon_k - \epsilon} (1 - n_{-\sigma}) c_{k\sigma}^\dagger d_\sigma - \text{H.c.} + \sum_{k\sigma} \frac{(\beta - \alpha)V/2}{\epsilon_k + \epsilon + U} n_{-\sigma} c_{k\sigma}^\dagger d_\sigma^\dagger - \text{H.c.} + \sum_{k\sigma} \frac{(\alpha + \beta)V/2}{\epsilon_k - \epsilon - U} n_{-\sigma} c_{k\sigma}^\dagger d_\sigma - \text{H.c.} \quad (44)$$

The effective Hamiltonian is very complicated. A number of terms are similar to those in the Schrieffer-Wolff transformation for the standard SIAM, Ref. 41, but with coefficients which depend on  $\alpha$  and  $\beta$  (and reproduce the standard values in the  $\alpha = \beta = 1$  limit). Furthermore, some magnetic anisotropy also arises. For example, the exchange-coupling terms can be written as

$$H_{\text{ex}} = \sum_{i \in \{x, y, z\}} \sum_{kk'} J_i (\Psi_{k'}^\dagger S_i \Psi_k) (\Psi_d^\dagger S_i \Psi_d), \quad (45)$$

where  $\mathbf{S} = \{S_x, S_y, S_z\} = (1/2)\boldsymbol{\sigma}$  are the Pauli matrices,

$$\Psi_k = \begin{pmatrix} c_{k\uparrow} \\ c_{k\downarrow} \end{pmatrix} \quad \text{and} \quad \Psi_d = \begin{pmatrix} d_\uparrow \\ d_\downarrow \end{pmatrix} \quad (46)$$

are field operators, and the effective Kondo exchange coupling coefficients  $J_i$  are equal to

$$J_x = J_z = \frac{V^2(\alpha + \beta)^2/2}{\epsilon_k - \epsilon} + \frac{V^2(\alpha - \beta)^2/2}{\epsilon_k + \epsilon} - \frac{V^2(\alpha + \beta)^2/2}{\epsilon_k - \epsilon - U} - \frac{V^2(\alpha - \beta)^2/2}{\epsilon_k + \epsilon + U}, \quad (47)$$

$$J_y = \frac{V^2(\alpha + \beta)^2}{\epsilon_k - \epsilon} - \frac{V^2(\alpha - \beta)^2}{\epsilon_k + \epsilon} - \frac{V^2(\alpha + \beta)^2}{\epsilon_k - \epsilon - U} + \frac{V^2(\alpha - \beta)^2}{\epsilon_k + \epsilon + U}.$$

Only in the  $\alpha = \beta = 1$  limit is the effective exchange scattering isotropic. At the particle-hole symmetric point we find

$$J_x = J_z = \alpha\beta \left( \frac{2V^2}{\epsilon_k + U/2} - \frac{2V^2}{\epsilon_k - U/2} \right), \quad (48)$$

$$J_y = \frac{(\alpha^2 + \beta^2)}{2} \left( \frac{2V^2}{\epsilon_k + U/2} - \frac{2V^2}{\epsilon_k - U/2} \right).$$

The direct  $s$ - $d$  interaction is

$$H_{\text{dir}} = \sum_{kk'} \left[ W - \frac{J_z}{4} (\Psi_d^\dagger \Psi_d) \right] (\Psi_{k'}^\dagger \Psi_k), \quad (49)$$

where

$$W = \frac{V^2(\alpha + \beta)^2/4}{\epsilon_k - \epsilon} + \frac{V^2(\alpha - \beta)^2/4}{\epsilon_k + \epsilon}. \quad (50)$$

The term which can be absorbed in the Hamiltonian  $H_0 = H_1 + H_3'$  can be written as

$$H'_0 = - \sum_{k\sigma} (W' + \frac{1}{2} J' n_{d,-\sigma}) n_{d,\sigma} \quad (51)$$

where

$$\begin{aligned} W' &= \frac{V^2(\alpha + \beta)^2/4}{\epsilon_k - \epsilon} - \frac{V^2(\alpha - \beta)^2/2}{\epsilon_k + \epsilon} \\ &\quad + \frac{V^2(\alpha - \beta)^2/4}{\epsilon_k + \epsilon + U} \\ J' &= - \frac{V^2(\alpha + \beta)^2/2}{\epsilon_k - \epsilon} + \frac{V^2(\alpha - \beta)^2}{\epsilon_k + \epsilon} \\ &\quad + \frac{V^2(\alpha + \beta)^2}{\epsilon_k - \epsilon - U} - \frac{V^2(\alpha - \beta)^2}{\epsilon_k + \epsilon U}. \end{aligned} \quad (52)$$

The two-particle hopping term is

$$H_{\text{ch}} = \frac{1}{4} \sum_{kk'\sigma} J_{2\text{h}} c_{k',-\sigma}^\dagger c_{k,\sigma}^\dagger d_\sigma d_{-\sigma} + \text{H.c.}, \quad (53)$$

with

$$J_{2\text{h}} = - \frac{V^2(\alpha + \beta)^2}{\epsilon_k - \epsilon} + \frac{V^2(\alpha + \beta)^2}{\epsilon_k - \epsilon - U}. \quad (54)$$

These are, however, not all the terms which appear in the effective Hamiltonian. Rather than enumerate all remaining contributions, we restrict our attention only to those which maintain the single occupancy of the impurity orbital. They can be written as:

$$H_{\text{si}} = \sum_{kk'} L \left( c_{k\uparrow}^\dagger c_{k'\downarrow}^\dagger - c_{k'\downarrow} c_{k\uparrow} \right) \left( d_\uparrow^\dagger d_\downarrow - d_\downarrow^\dagger d_\uparrow \right) \quad (55)$$

with

$$\begin{aligned} L &= \frac{V^2(\beta^2 - \alpha^2)/8}{\epsilon_k - \epsilon} + \frac{V^2(\alpha^2 - \beta^2)/8}{\epsilon_k + \epsilon} \\ &\quad + \frac{V^2(\beta^2 - \alpha^2)/8}{\epsilon_k - \epsilon - U} + \frac{V^2(\beta^2 - \alpha^2)/8}{\epsilon_k + \epsilon + U}. \end{aligned} \quad (56)$$

We now discuss the  $\alpha = 0, \beta = 1$  limit, which is relevant for discussing an Anderson impurity coupled to the edge states of a helical topological superconductor. The most important terms in the effective Hamiltonian are those which affect the impurity spin degrees of freedom:

$$H_{\text{eff}} = H_{\text{ex}} + H_{\text{si}}. \quad (57)$$

The exchange coupling constants are anisotropic:

$$\begin{aligned} J_{x/z} &= \frac{V^2/2}{\epsilon_k - \epsilon} + \frac{V^2/2}{\epsilon_k + \epsilon} - \frac{V^2/2}{\epsilon_k - \epsilon - U} - \frac{V^2/2}{\epsilon_k + \epsilon + U}, \\ J_y &= \frac{V^2/2}{\epsilon_k - \epsilon} - \frac{V^2/2}{\epsilon_k + \epsilon} - \frac{V^2/2}{\epsilon_k - \epsilon - U} + \frac{V^2/2}{\epsilon_k + \epsilon + U}. \end{aligned} \quad (58)$$

At the particle-hole symmetric point this simplifies to

$$\begin{aligned} J_{x/z} &= 0, \\ J_y &= \frac{4V^2U}{U^2 - 4\epsilon_k} \approx \frac{4V^2}{U}, \end{aligned} \quad (59)$$

where we have used  $\epsilon_k \rightarrow 0$ . Within the same approximation, we also have

$$L \approx \frac{V^2}{U}. \quad (60)$$

We combine all terms and write

$$\begin{aligned} H_{\text{eff}} &= \frac{V^2}{U} \left[ 4S_y s_y + (I^+ - I^-) (s^+ - s^-) \right] \\ &= \frac{4V^2}{U} (S_y - I_y) s_y. \end{aligned} \quad (61)$$

Here upper-case operators  $I$  and  $S$  correspond to the conduction-band isospin and spin, while the lower-case operators are those of the impurity. Furthermore,  $I^+ = I_x + iI_y$ , etc. We thus conclude that in the large- $U$  limit, the impurity spin degree of freedom couples to a mixed  $S_y - I_y$  mode, which can be expressed in terms of a single Majorana channel. This result was postulated without derivation in Ref. 27. It is important to note, however, that the derivation and the effective model only make sense in the large- $U$  limit, i.e., the coupling constant  $J_K = 4V^2/U$  verifies  $J_K \ll V \ll U$ . The phase transition discussed in Ref. 27 occurs at a value of  $\rho J_K \sim O(1)$  which is therefore unphysical. Thus we conclude that such phase transition is not expected in real magnetic impurities coupled to topological superconductors.

## VI. CONCLUSION

We have studied the properties of the modified single-impurity Anderson model where the impurity couples only to half of the degrees of freedom of standard fermionic particles in the conduction-band continuum, i.e., to Majorana fermion channels. We have shown that the model is related to the two-level resonant model with attractive charge-charge interaction and to the (antiferromagnetic or ferromagnetic) anisotropic Kondo model. Two different stable low-temperature fixed points have been identified: one corresponds to magnetic impurities and is characterized by residual magnetic moment and entropy, the other corresponds to non-magnetic impurities with no residual degrees of freedom. The phase diagram separating these two regimes has been established. We have also shown that the magnetic field always destabilizes the magnetic fixed point, however the response is strongly anisotropic.

For magnetic impurities, the residual degree of freedom corresponds to the operator  $s_y + i s_z$ . While the charge degrees of freedom are quenched due to electron-electron repulsion, for impurities which are not in the extreme Kondo limit ( $U \gg \Gamma$ ) the isospin degree of freedom determines the quantitative aspects of the problem. For this reason, we have shown that it is important to properly map the original Anderson model to an effective Kondo model, rather than start by postulating a Kondo-like model.

Finally, we would like to stress that the predictions we have made can be put to an experimental test since dynamical magnetic susceptibility is in principle measurable experimentally.

### ACKNOWLEDGMENTS

R. Ž. acknowledges the support of the Slovenian Research Agency (ARRS) under Grant No. Z1-2058 and Program P1-0044.

### Appendix A: Complex hybridization matrix elements

For completeness, we now study the case of general complex and spin-dependent hybridization matrix elements, that is, the coupling Hamiltonian is written as

$$H_2 = \sum_{k\sigma} (V_\sigma \eta_{k\sigma} d_\sigma + V_\sigma^* d_\sigma^\dagger \eta_{k\sigma}), \quad (\text{A1})$$

where  $V_\sigma$  is a complex number,  $V_\sigma = |V_\sigma| \exp(i\theta_\sigma)$ .

Introducing  $\eta_{i\sigma}$  as in Eq. (6), we obtain

$$H_2 = \sum_{k\sigma} |V_\sigma| \sqrt{2} i (\cos \theta_\sigma \eta_{k\sigma} \eta_{2\sigma} + \sin \theta_\sigma \eta_{k\sigma} \eta_{1\sigma}). \quad (\text{A2})$$

We now perform a change of basis to

$$\begin{aligned} \xi_{1\sigma} &= \cos \theta_\sigma \eta_{1\sigma} - \sin \theta_\sigma \eta_{2\sigma}, \\ \xi_{2\sigma} &= \sin \theta_\sigma \eta_{1\sigma} + \cos \theta_\sigma \eta_{2\sigma}, \end{aligned} \quad (\text{A3})$$

and obtain

$$H_2 = \sum_{k\sigma} |V_\sigma| \sqrt{2} i \eta_{k\sigma} \xi_{2\sigma}. \quad (\text{A4})$$

Thus we find, again, that only two Majorana local modes  $\xi_{2\sigma}$  are coupled to the impurity, while the remaining two modes  $\xi_{1\sigma}$  are decoupled. If  $\xi_{1\uparrow} \xi_{1\downarrow}$  is rewritten in terms of the original Dirac operators, it is found that it corresponds to a linear combination of spin and isospin operators in the  $(xy)$  plane:

$$\begin{aligned} i\xi_{1\downarrow} \xi_{1\uparrow} &= \sin(\theta_\downarrow - \theta_\uparrow) s_x + \cos(\theta_\downarrow - \theta_\uparrow) s_y \\ &\quad - \sin(\theta_\uparrow + \theta_\downarrow) i_x + \cos(\theta_\uparrow + \theta_\downarrow) i_y. \end{aligned} \quad (\text{A5})$$

In the absence of spin-dependence, i.e., for  $\theta_\uparrow = \theta_\downarrow$ , we obtain

$$i\xi_{1\downarrow} \xi_{1\uparrow} = s_y - \sin(2\theta) i_x + \cos(2\theta) i_y, \quad (\text{A6})$$

which implies that the privileged ‘‘longitudinal’’ magnetic axis is still along the  $y$  direction, however the privileged isospin axis deviates by an angle of  $2\theta$  from the  $y$ -axis. For  $\theta_\uparrow = \theta_\downarrow = 0$  we recover the result from the main text,

$$i\xi_{1\downarrow} \xi_{1\uparrow} = s_y + i_y. \quad (\text{A7})$$

We remind the reader that the  $z$ -axis is defined by the spin polarization of the Majorana edge modes. The  $x$  and  $y$ -axes are thus always defined relative to this spin quantization axis.

- 
- <sup>1</sup> F. Wilczek, Nat. Phys. **5**, 614 (2009).  
<sup>2</sup> A. Stern, Nature **464**, 187 (2010).  
<sup>3</sup> M. Franz, Physics **3**, 24 (2010).  
<sup>4</sup> X.-L. Qi and S.-C. Zhang, *Topological insulators and superconductors*, arXiv:1008.2026 (2010).  
<sup>5</sup> M. Z. Hasan and C. L. Kane, Rev. Mod. Phys. **82**, 3045 (2010).  
<sup>6</sup> C. L. Kane and E. J. Mele, Phys. Rev. Lett. **95**, 146802 (2005).  
<sup>7</sup> L. Fu and C. L. Kane, Phys. Rev. B **74**, 195312 (2006).  
<sup>8</sup> B. A. Bernevig and S.-C. Zhang, Phys. Rev. Lett. **96**, 106802 (2006).  
<sup>9</sup> J. E. Moore and L. Balents, Phys. Rev. B **75**, 121306(R) (2007).  
<sup>10</sup> B. A. Bernevig, T. L. Hughes, and S.-C. Zhang, Science **314**, 1757 (2006).  
<sup>11</sup> M. König et al., Science **318**, 766 (2007).  
<sup>12</sup> L. Fu and C. L. Kane, Phys. Rev. Lett. **100**, 096407 (2008).  
<sup>13</sup> L. Fu and C. L. Kane, Phys. Rev. Lett. **102**, 216403 (2009).  
<sup>14</sup> J. D. Sau, R. M. Lutchyn, S. Tewari, and S. Das Sarma, Phys. Rev. Lett. **104**, 040502 (2010).  
<sup>15</sup> J. D. Sau, R. M. Lutchyn, S. Tewari, T. D. Stanescu, and S. Das Sarma, Phys. Rev. B **82**, 214509 (2010).  
<sup>16</sup> L. Fu and C. L. Kane, Phys. Rev. B **79**, 161408(R) (2009).  
<sup>17</sup> Y. Tanaka, T. Yokoyama and N. Nagaosa, Phys. Rev. Lett. **103**, 107002 (2009).  
<sup>18</sup> X.-L. Qi, T. L. Hughes, S. Raghy and S.-C. Zhang, Phys. Rev. Lett. **102**, 187001 (2009).  
<sup>19</sup> R. Roy, *Topological superfluids with time reversal symmetry*, arXiv:0803.2868 (2008).  
<sup>20</sup> M. Sato and S. Fujimoto, Phys. Rev. B **79**, 094504 (2009).  
<sup>21</sup> X.-L. Qi, T. L. Hughes and S.-C. Zhang, Phys. Rev. B **82**, 184516 (2010).  
<sup>22</sup> S. Gangadharaiah, B. Braunecker, P. Simon, and D. Loss, Phys. Rev. Lett. **107**, 036801 (2011).  
<sup>23</sup> E. M. Stoudenmire, J. Alicea, O. A. Starykh, and M. P. A. Fisher, arXiv:1104.5493 (2011).  
<sup>24</sup> A. R. Akhmerov, J. P. Dahlhaus, F. Hassler, M. Wimmer, and C. W. J. Beenakker, Phys. Rev. Lett. **106**, 057001 (2011).  
<sup>25</sup> A. C. Potter and P. A. Lee, Phys. Rev. B **83**, 184520 (2011).  
<sup>26</sup> P. W. Brouwer, M. Duckheim, A. Romito, and F. von Oppen, arXiv:1103.2746 (2011).  
<sup>27</sup> R. Shindou, A. Furusaki, and N. Nagaosa, Phys. Rev. B **82**, 180505 (2010).  
<sup>28</sup> M. Goldstein and R. Berkovits, New J. Phys. **9**, 118 (2007).  
<sup>29</sup> C. Karrasch, T. Hecht, A. Weichselbaum, J. von Delft, Y. Oreg, and V. Meden, New J. Phys. **9**, 123 (2007).  
<sup>30</sup> V. Kashcheyevs, C. Karrasch, T. Hecht, A. Weichselbaum, V. Meden, and A. Schiller, Phys. Rev. Lett. **102**, 136805 (2009).  
<sup>31</sup> M. Goldstein, R. Berkovits, and Y. Gefen, Phys. Rev. Lett. **104**, 226805 (2010).  
<sup>32</sup> P. Schlottmann, Phys. Rev. B **22**, 622 (1980).  
<sup>33</sup> T. Giamarchi, C. Varma, A. E. Ruckenstein, and P. Nozières, Phys. Rev. Lett. **70**, 3967 (1993).  
<sup>34</sup> P. W. Anderson, G. Yuval, and D. R. Hamann, Phys. Rev. B **1**,

- 4464 (1970).
- <sup>35</sup> K. G. Wilson, Rev. Mod. Phys. **47**, 773 (1975).
- <sup>36</sup> H. R. Krishnamurthy, J. W. Wilkins, and K. G. Wilson, Phys. Rev. B **21**, 1003 (1980).
- <sup>37</sup> R. Bulla, T. Costi, and T. Pruschke, Rev. Mod. Phys. **80**, 395 (2008).
- <sup>38</sup> R. Žitko, Phys. Rev. B **83**, 195137 (2011).
- <sup>39</sup> H. R. Krishnamurthy, J. W. Wilkins, and K. G. Wilson, Phys. Rev. B **21**, 1044 (1980).
- <sup>40</sup> A.C. Hewson, *The Kondo Problem to Heavy Fermions*, Cambridge University Press, Cambridge, UK, (1993).
- <sup>41</sup> J. R. Schrieffer and P. A. Wolff, Phys. Rev. **149**, 491 (1966).
- <sup>42</sup> S. Bravyi, D. DiVincenzo, and D. Loss, arXiv:1004.3791.